Amorphous $Mo_aZr_{0.8}O_x$-500 catalyzed selective oxidation of sulfides to sulfoxides mediated by $^1O_2$ from direct heterolytic cleavage H_2O_2

Tong Li[a], Jiaheng Qin[a], Xueyao Zhang[c], Xiaoqi Tang[a], Mingzhe Lv[a], Weiwen Mao[a], Linkun Dong[a], Tongtong Fan[a], Yu Long*[a, b], Jiantai Ma*[a, b]

[a] State Key Laboratory of Applied Organic Chemistry (SKLAOC), Gansu Provincial Engineering Laboratory for Chemical Catalysis, College of Chemistry and Chemical Engineering, Lanzhou University, Lanzhou 730000, P. R. China.

[b] MOE Frontiers Science Center for Rare Isotopes, Lanzhou University, Lanzhou 730000, P. R. China.

[c] School of Life Sciences, Lanzhou University, Lanzhou 730000, P. R. China.

* E-mail: longyu@lzu.edu.cn (Yu Long), majiantai@lzu.edu.cn (Jiantai Ma)

Experimental details

1. Materials

Zirconium hydroxide ($Zr(OH)_4$, 97%), ammonium molybdate tetrahydrate ($(NH_4)_6Mo_7O_{24}\cdot 4H_2O$, 99%) and Molybdenum trioxide (MoO_3, 99.5%) were purchased commercially from Macklin. Methyl phenyl sulfide, 4-Methoxyphenyl methyl sulfide, 4-Aminophenyl methyl sulfide, 4-Fluorophenyl methyl sulfide, 4-Chlorophenyl methyl sulfide, 2-Chlorophenyl methyl sulfide, 4-(Methylthio)benzaldehyde, 4-Acetylphenyl methyl sulfide, Diphenyl sulfide, Diethyl sulfide, Dipropyl sulfide, Dibutyl sulfide, 2-Chloroethyl ethyl sulfide were purchased commercially from Macklin. 4-Nitrophenyl methyl sulfide and (4-Methylphenyl) methyl sulfide were purchased commercially from Leyan. 4-(Methylthio)benzyl alcohol and phenyl benzyl sulfide were purchased commercially from Bidepharmatech. Ammonium metatungstate ($(NH_4)_6H_2W_{12}O_{40}\cdot xH_2O$) and Nickel chloride hexahydrate ($NiCl_2\cdot 6H_2O$) were purchased commercially from Aladdin. Ammonium chromate ($(NH_4)_2CrO_4$), lanthanum nitrate hexahydrate ($La(NO_3)_3\cdot 6H_2O$), cerium chloride hexahydrate($CeCl_3\cdot 6H_2O$) , cobalt chloride hexahydrate($CoCl_2\cdot 6H_2O$), 1,3-diphenylisobenzofuran (DPBF, 97%) and nitrotetrazolium blue chloride (NBT, 98%) were purchased commercially from Macklin. Ferric nitrate nonahydrate ($Fe(NO_3)_3\cdot 9H_2O$) and calcium hydroxide ($Ca(OH)_2$) were purchased commercially from Kelong. Cupric nitrate ($Cu(NO_3)_2$) and aluminum hydroxide ($Al(OH)_3$) were purchased commercially from Damao. All solvents were analytically pure and not further purified.

2. Characterization

Gas chromatography (GC) analysis was conducted on an Agilent GC 8090 instrument equipped with a flame ionization detector (FID) and an HP-5MS capillary column (30 m, 0.25 mm i.d., 0.25 μm film thicknesses) using nitrogen as the carrier gas. Gas chromatography-mass spectrometry (GC–MS) analysis was performed on an Agilent 5977C GC/MSD instrument with an Agilent HP-5975 with triple-axis detector and HP-5 capillary column using helium as the carrier gas.

The crystal structure of the catalysts was investigated by powder X-ray diffraction (XRD) using a Rigaku D/max-2400 diffractometer with Cu-Kα radiation. The samples were scanned at a rate of 5° min^{-1} at room temperature.

The morphological characteristics of the catalysts were analyzed using scanning electron microscopy (SEM, S-6800) and transmission electron microscopy (TEM, FEI Talos F200s).

The surface and structural properties of the samples were investigated using the N_2 adsorption-desorption isotherm (ASAP2020) at liquid nitrogen temperature (77 K). Prior to measurement, all samples were degassed under vacuum at 473 K for 6 h. The specific surface area of the catalysts was determined by the Brunel-Emmett-Teller (BET) method. Pore size distributions were calculated from the adsorption curves using non-local density functional theory (NLDFT).

X-ray photoelectron spectroscopy (XPS) was conducted on a PH-5702 instrument with an anode of Mg Kα (hυ = 1253.6 eV) and a base pressure of 5×10^{-8} mbar. The binding energy (BE) was adjusted for the C1s peak of carbon at 284.6 eV.

Raman spectroscopy was recorded on a Laser Micro-Raman spectrometer system using a 532 nm wavelength laser at room temperature.

A series of programmed thermal desorption (TPD) experiments were conducted on an Auto Chem II 2720 chemisorbent manufactured by Micromeritics, USA, utilizing a TCD (Thermal Conductivity Detector). For the NH_3- and CO_2-TPD experiments, 50 mg of the catalyst was purged under a stream of argon (25 mL·min^{-1}) at 100 °C for 1 h, and then cooled to room temperature. Following this, the sample was adsorbed at 30°C for 30 minutes in 10% NH_3/Ar or 10% CO_2/Ar. The temperature was then increased to

950 °C at a ramp rate of 10 °C min^{-1}. Subsequently, the catalysts were maintained at a temperature of 950 °C for a period of 30 minutes.

Infrared testing was conducted using potassium bromide (KBr) and the catalysts by pressing approximately 5 mg of the samples with 100 mg of KBr. Surface chemical bonding of the samples was then tested using Fourier Transform Infrared Spectroscopy (FT-IR, Nicolet NEXUS 670). The spectra were obtained after 32 scans of each sample, with a resolution of 4 cm^{-1} over a range of 400-4000 cm^{-1}.

The electron paramagnetic resonance (EPR) spectra were collected on a ER200DSRC10/12 EPR spectrometer (Bruker, Germany).

The objective of this study is to investigate the detection of $^1O_2$ and $\bullet O_2^-$ using ultraviolet-visible (UV-Vis) absorption spectroscopy (UV-4802, UNICO (SHANGHAI) INSTRUMENT).

The Zr ion concentration was analyzed by an inductively coupled plasma emission spectrometer (ICP-OES).

3. General procedures for oxidation sulfides.

The oxidation of all thioethers was conducted in a 25 ml reaction tube. The procedure was as follows: 20 mg of catalyst, 1 mmol of sulfides, and 3 mL of methanol were sequentially added to the reaction tube and mixed well with stirring for a period of time at 30℃. Subsequently, 110 μL (1.1 mmol) of a 30% H_2O_2 solution was added using a microsyringe, and the reaction was carried out for 30 minutes. At the conclusion of the reaction, the reaction mixture was filtered through a nylon filter membrane with a pore size of 0.22 μm. The conversion and selectivity were determined using gas chromatography (GC) with a flame ionization detector, while the final product was determined using gas chromatography-mass spectrometry (GC-MS), with biphenyl serving as the internal standard.

The details of the conversion and selectivity calculations are as follows:

$$m_i^* = f_i * A_i^*$$

$$m_s^* = f_s * A_s^*$$

$$f_{is} = \frac{f_i}{f_s} = \frac{m_i^* * A_s^*}{m_s^* * A_i^*}$$

$$m_i = \frac{f_i * A_i}{f_s * A_s} \cdot m_s = f_{is} \cdot \frac{A_i}{A_s} \cdot m_s$$

$$n_i = \frac{m_i}{M_i}$$

m_i^*-Mass of sulfide, sulfoxide and sulfone in standard solution.

m_s^*-Mass of internal standard in standard solution(biphenyl).

A_i^*-Gas chromatography peak area of sulfide, sulfoxide, sulfone in standard solution.

A_s^*-Gas chromatography peak area of internal standard (biphenyl) in standard solution.

m_i-Mass of sulfide, sulfoxide and sulfone in reaction solution.

m_s-Mass of internal standard in reaction solution(biphenyl) in reaction solution.

A_i-Gas chromatography peak area of sulfide, sulfoxide, sulfone in reaction solution.

A_s-Gas chromatography peak area of internal standard (biphenyl) in reaction solution.

f_{is}- The relative correction factor of sulfide, sulfoxide and sulfone.

$n_{i,sulfide}$, $n_{i,sulfoxide}$ and $n_{i,sulfone}$ are calculated from the above equation. n is molar amount of sulfide before reaction (1 mmol)

$$Conversion = \frac{n - n_{i,sulfide}}{n} \times 100\%$$

$$Selectivity = \frac{n_{i,sulfoxide}}{n_{i,sulfoxide} + n_{i,sulfone}} \times 100\%$$

$$Carbon\ balance = \frac{n_{i,sulfide} + n_{i,sulfoxide} + n_{i,sulfone}}{n} \times 100\%$$

4. Procedure for the catalyst recycling

Once the reaction had reached completion, the contents of the reaction tube were transferred to a centrifuge tube. Centrifugation at 10,000 rpm for 3 min was then performed, after which a quantity of the supernatant was filtered through a nylon filter membrane with a pore size of 0.22 microns into a gas phase vial for gas phase analysis. Subsequently, the sample was washed by centrifugation at 10,000 rpm for 3 min using anhydrous ethanol on three occasions. It was then dried in an oven at 60 ℃ for one hour and then roasted in a muffle furnace at 300 ℃ for one hour. It was cooled to room temperature and used for the next run.

5. The kinetic measurements.

5.1 The kinetic experiments procedure for $Mo_{0.10}Zr_{0.8}O_x$-500 is as follows:

1 mmol of methyl phenyl sulfide, 20 mg of $Mo_{0.10}Zr_{0.8}O_x$-500, and 3 mL of methanol were combined and stirred at the test temperature for several minutes to achieve equilibrium. Subsequently, 110 μL of 30% H_2O_2 solution were added. Following a 30-second reaction period, a quantity of the reaction solution was filtered using a 0.22-micron filter membrane into a gas phase vial for analysis. To determine the initial reaction rate at different reaction times, the above procedure was repeated while maintaining the reaction temperature. Samples were taken and analyzed at 60s, 90s, 120s, and 150s. Subsequently, the experimental temperature was varied, and the aforementioned methodology was repeated to assess the kinetics at 298K, 301K, 303K, 306K, and 308K, respectively.

5.2 The kinetic tests procedure for $Mo_{0.10}/Zr_{0.8}O_x$-500-DIM, MoO_3, and ZrO_2 is as follows:

The procedure remains the same as for $Mo_{0.10}Zr_{0.8}O_x$-500, with the exception that the starting time, the length of the interval, and the reaction temperature are not the same as for $Mo_{0.10}Zr_{0.8}O_x$-500.

Specifically, the $Mo_{0.10}/Zr_{0.8}O_x$-500-DIM was reacted at temperatures of 298K, 303K, 308K, 313K, and 318K, respectively, with a starting reaction time of 60 s at each temperature. Samples were taken and analyzed at 60 s, 120 s, 180 s, 240 s, and 300 s, respectively.

MoO_3 was subjected to kinetic testing at temperatures of 303K, 308K, 313K, 318K, and 323K, with an onset time of 60s at each temperature. Additionally, samples were collected and analyzed at 60s, 120s, 180s, 240s, and 300s, respectively.

The testing temperature of ZrO_2 was identical to that of $Mo_{0.10}/Zr_{0.8}O_x$-500-DIM, and the initial reaction time was 180 seconds. Samples were collected and analyzed at 180 seconds, 360 seconds, 540 seconds, 720 seconds, and 900 seconds, respectively.

The details of the calculations are as follows:

The first order reaction kinetic equation allows for the calculation of the reaction rate constant, k (s^{-1}). The kinetic equation for the first order reaction is as follows:

$$\ln \frac{C_0}{C} = kt$$

The Arrhenius equation is defined as follows:

$$k = Ae^{-E_a/RT}$$

The apparent activation energy of the reaction can be calculated using the Arrhenius equation. In particular, a graph is plotted with lnk as the vertical coordinate and 1/T(K) as the horizontal coordinate. The specific value of the apparent activation energy can then be derived from the resulting slope.

$$\ln k = -\frac{E_a}{RT} + \ln A$$

Table S1 The catalyst reaction time and solvent quantity screening.

Entry	Time (min)	Methanol (mL)	Conv.(%)[b]	Select.(%)[b]
1	15	3	83.2	93.9
2	20	3	95.6	93.8
3	30	2	97.4	93.1
4	30	4	95.0	93.3
5	30	5	95.7	93.5

[a] Reaction conditions: sulfide (1 mM), $Mo_{0.10}/ZrO_2$-500 (20 mg), H_2O_2 (1.1 mM), 30 ℃, 30 min. [b] Conversions and selectivity were determined using gas chromatography, with biphenyl serving as the internal standard.

Table S2 Screen various solvent types.

Entry	Solvent	Conv.(%)[c]	Select.(%)[c]
1	Ethanol	84.8	92.7
2	n-propanol	87	94.3
3	i-propanol	79.1	94.8
4	n-butanol	93.6	93.7
5	i-butanol	96.6	93.1
6	n-Hexyl alcohol	91.7	92.3
7	Acetonitrile	84.2	81.4
8	THF	34.1	82.2
9	Acetone	56.2	81.5
10	Ethyl acetate	72.5	87.7
11	Cyclohexanone	60	86.8
12	1,4-Dioxane	38.3	95.7
13[b]	H_2O	47.6	93.5

[a] Reaction conditions: sulfide (1 mM), Catalyst (20 mg), Solvent (3 mL), H_2O_2 (1.1 mM), 30 ℃, 30 min. [b] The extraction procedure was conducted utilizing ethyl acetate. [c] Conversions and selectivity were determined using gas chromatography, with biphenyl serving as the internal standard.

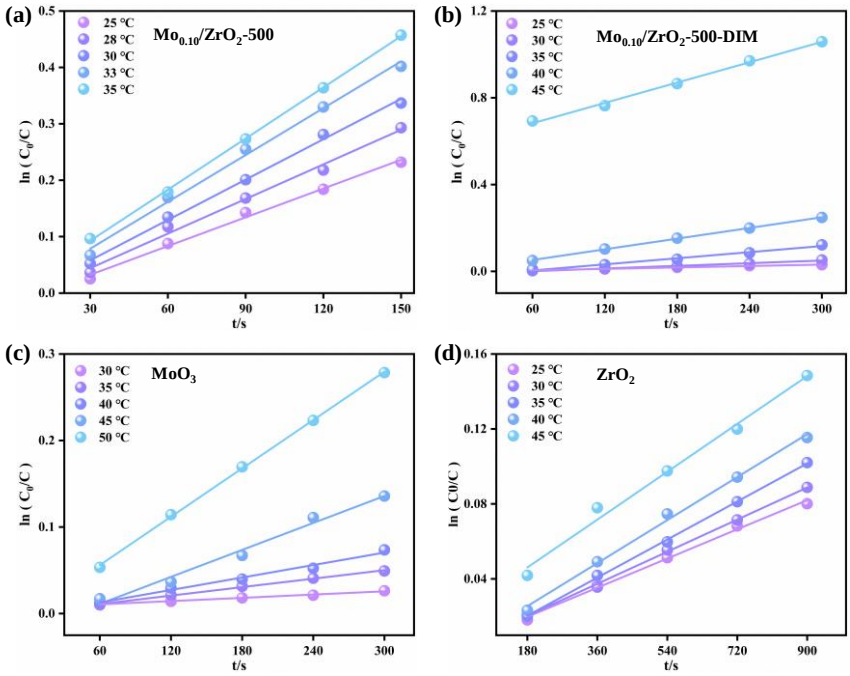

Figure S1. The kinetic experiments of $Mo_{0.10}Zr_{0.8}O_x$-500 (a), $Mo_{0.10}/Zr_{0.8}O_x$-500-DIM (b), MoO_3 (c) and ZrO_2 (d).

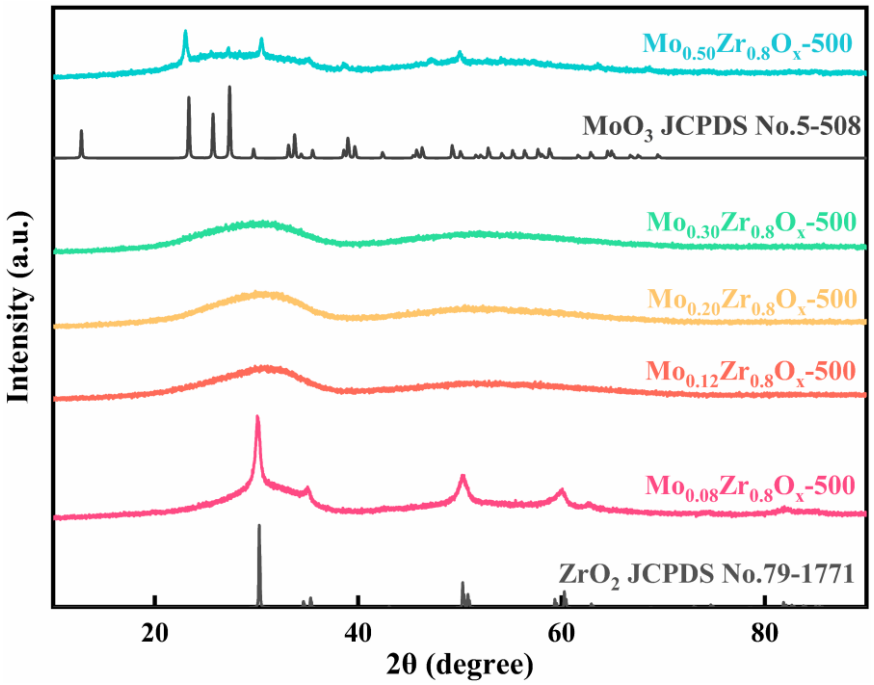

Figure S2. XRD patterns of $Mo_{0.08}Zr_{0.8}O_x$-500, $Mo_{0.12}Zr_{0.8}O_x$-500, $Mo_{0.20}Zr_{0.8}O_x$-500, $Mo_{0.30}Zr_{0.8}O_x$-500, $Mo_{0.50}Zr_{0.8}O_x$-500.

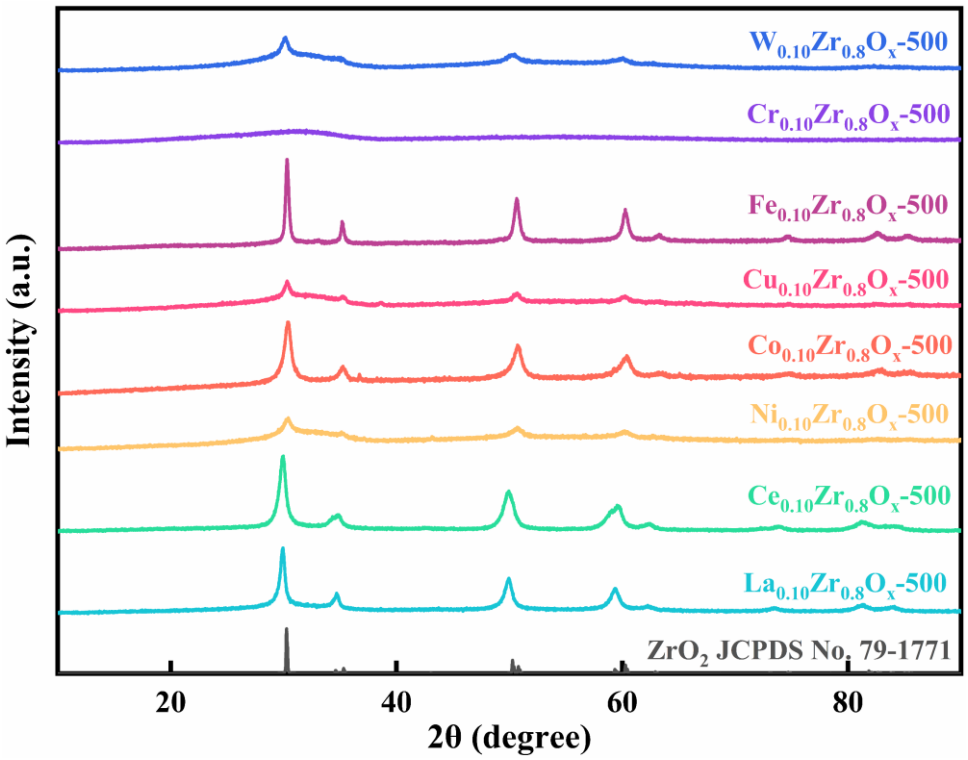

Figure S3. XRD patterns of $W_{0.10}Zr_{0.8}O_x$-500, $CrZr_{0.8}O_x$-500, $FeZr_{0.8}O_x$-500, $CuZr_{0.8}O_x$-500, $CoZr_{0.8}O_x$-500, $NiZr_{0.8}O_x$-500, $CeZr_{0.8}O_x$-500, $LaZr_{0.8}O_x$-500.

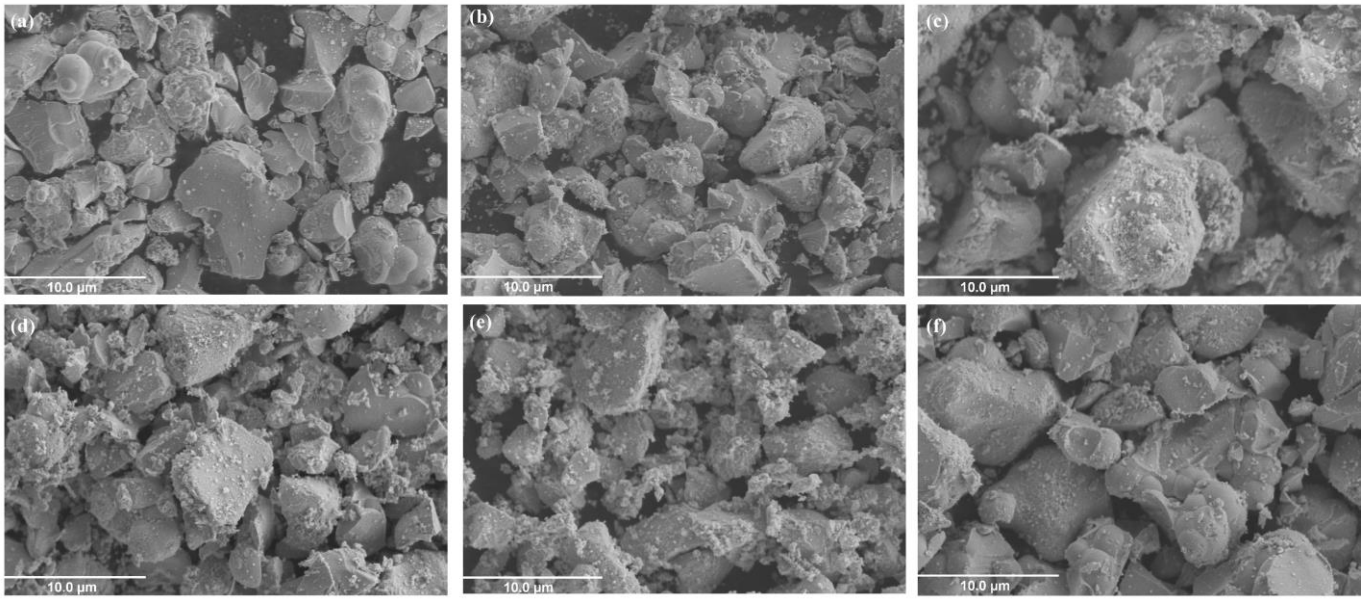

Figure S4. SEM images of $Mo_{0.08}Zr_{0.8}O_x$-500, $Mo_{0.10}Zr_{0.8}O_x$-500, $Mo_{0.12}Zr_{0.8}O_x$-500, $Mo_{0.20}Zr_{0.8}O_x$-500, $Mo_{0.30}Zr_{0.8}O_x$-500, $Mo_{0.50}Zr_{0.8}O_x$-500.

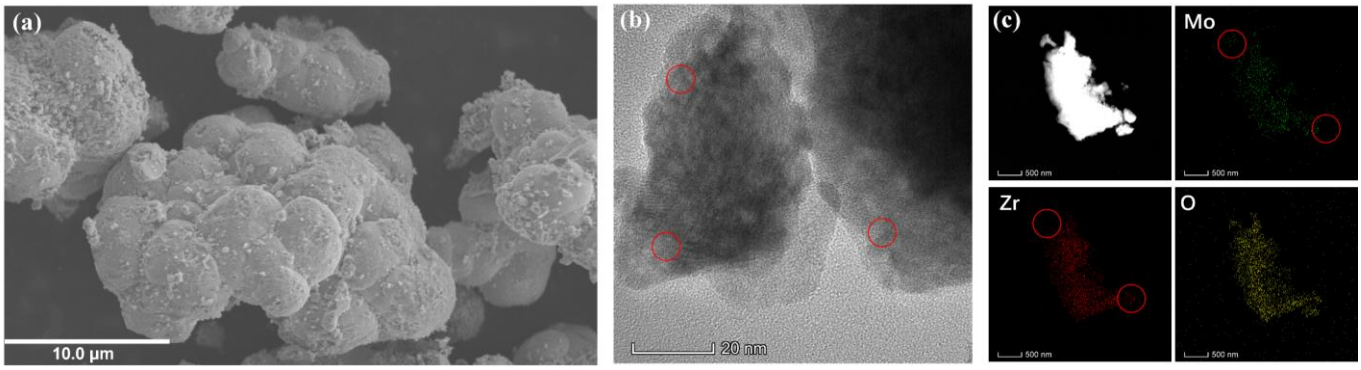

Figure S5. (a) SEM image of $Mo_{0.10}/Zr_{0.8}O_x$-500-DIM. (b) and (c) TEM image, HADDF-STEM image and EDX elemental mappings of $Mo_{0.10}/Zr_{0.8}O_x$-500-DIM.

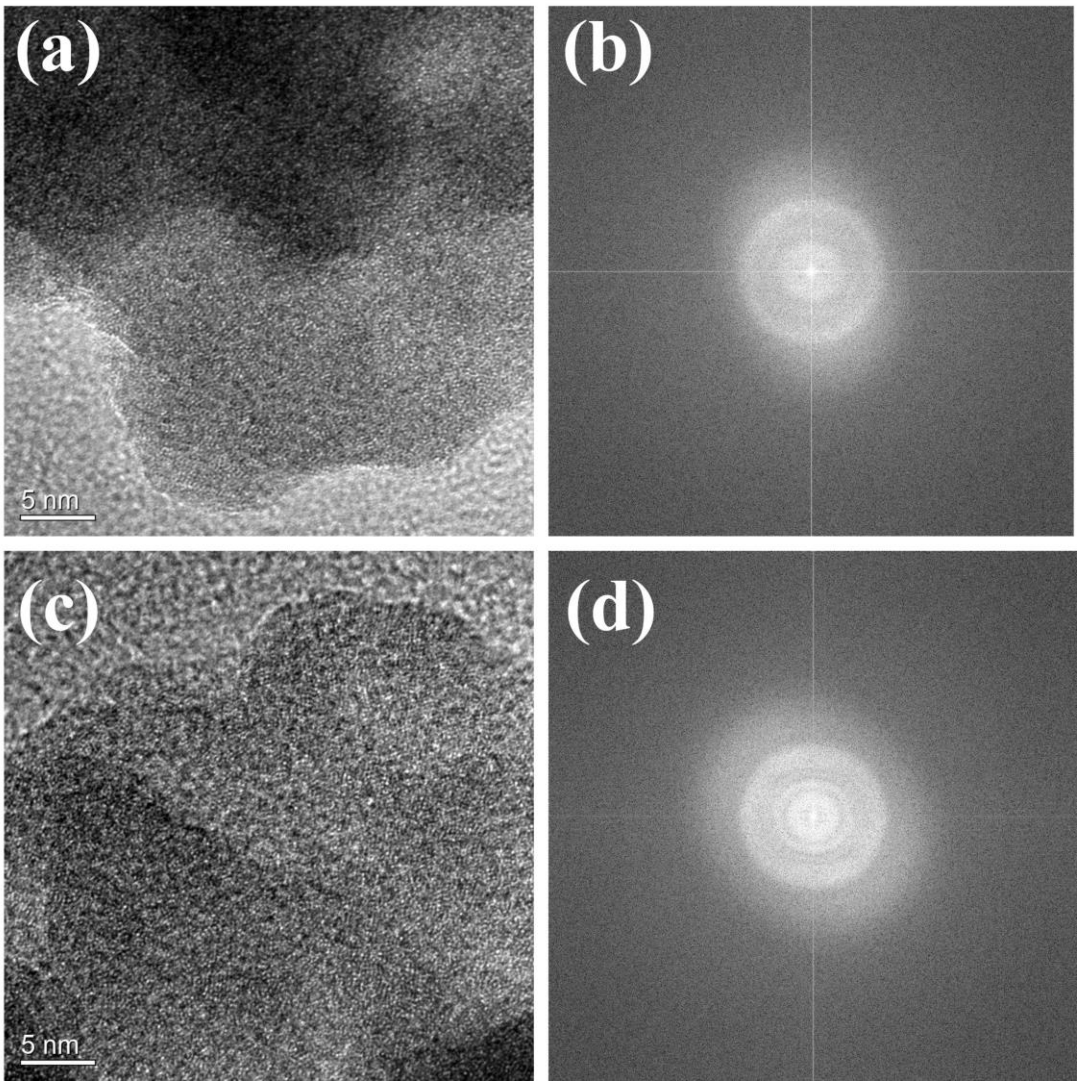

Figure S6. (a)-(d) HR-TEM image and electron diffraction of $Mo_{0.10}Zr_{0.8}O_x$-500 in the selected other area.

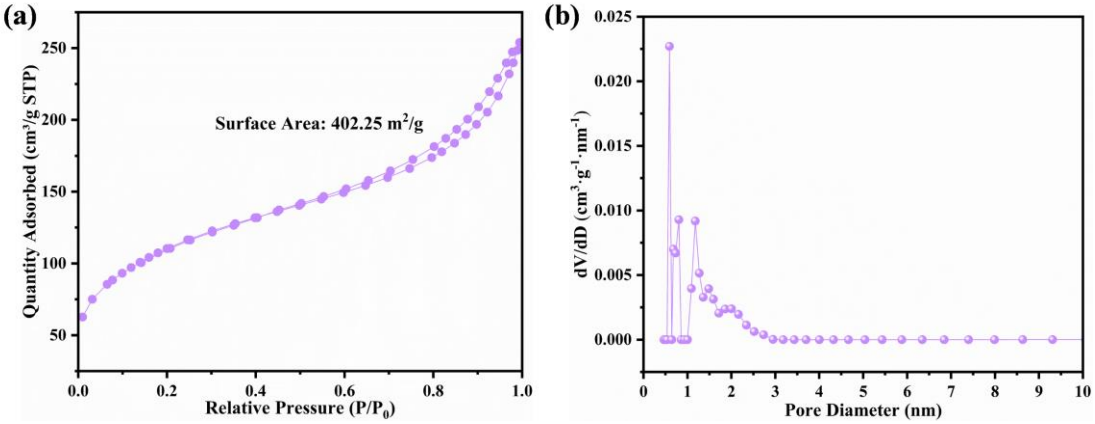

Figure S7. N_2 adsorption-desorption isotherms and the pore size distributions of $Zr(OH)_4$.

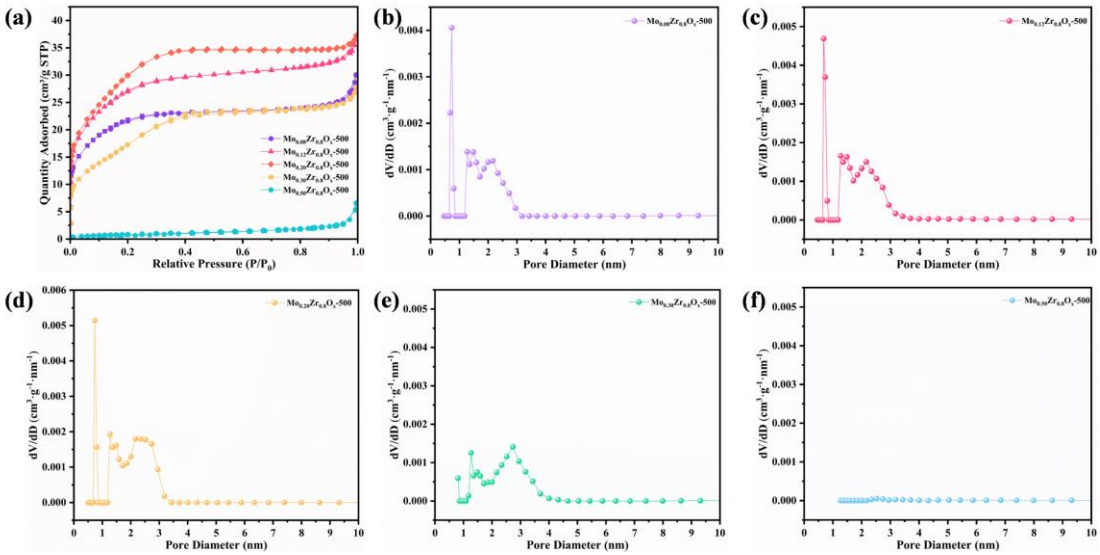

Figure S8. N_2 adsorption-desorption isotherms and the pore size distributions of $Mo_{0.08}Zr_{0.8}O_x$-500, $Mo_{0.12}Zr_{0.8}O_x$-500, $Mo_{0.20}Zr_{0.8}O_x$-500, $Mo_{0.30}Zr_{0.8}O_x$-500, $Mo_{0.50}Zr_{0.8}O_x$-500.

Table S3 Surface properties of catalysts.

Catalysts	BET Specific Surface Area (m^2/g)	BJH Desorption average pore diameter (nm)
$Mo_{0.08}Zr_{0.8}O_x$-500	74.82	4.45
$Mo_{0.10}Zr_{0.8}O_x$-500	114.1	4.11
$Mo_{0.12}Zr_{0.8}O_x$-500	95.03	3.77
$Mo_{0.20}Zr_{0.8}O_x$-500	110.07	2.61
$Mo_{0.30}Zr_{0.8}O_x$-500	66.15	2.94
$Mo_{0.50}Zr_{0.8}O_x$-500	2.73	7.58
$Mo_{0.10}/Zr_{0.8}O_x$-500-DIM	1.18	12.5
MoO_3	1.27	19.08
ZrO_2	40.87	3.3

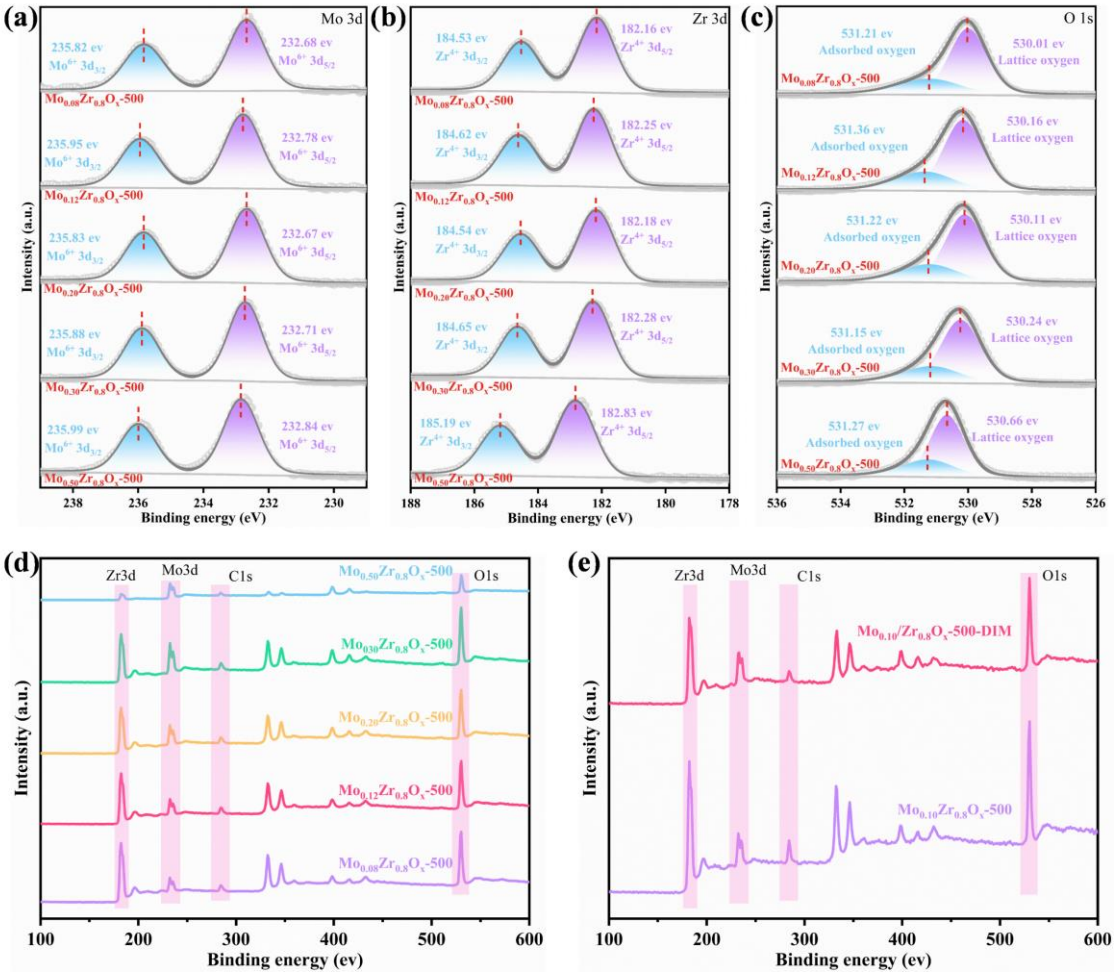

Figure S9. The deconvolution results of XPS spectra of $Mo_{0.08}Zr_{0.8}O_x$-500, $Mo_{0.12}Zr_{0.8}O_x$-500, $Mo_{0.20}Zr_{0.8}O_x$-500, $Mo_{0.30}Zr_{0.8}O_x$-500, $Mo_{0.50}Zr_{0.8}O_x$-500 for Mo 3d (a), Zr 3d (b) and O 1s (c). (d) and (e) XPS survey pattern of $Mo_{0.08}Zr_{0.8}O_x$-500, $Mo_{0.10}Zr_{0.8}O_x$-500, $Mo_{0.12}Zr_{0.8}O_x$-500, $Mo_{0.20}Zr_{0.8}O_x$-500, $Mo_{0.30}Zr_{0.8}O_x$-500, $Mo_{0.50}Zr_{0.8}O_x$-500 and $Mo_{0.10}/Zr_{0.8}O_x$-500-DIM.

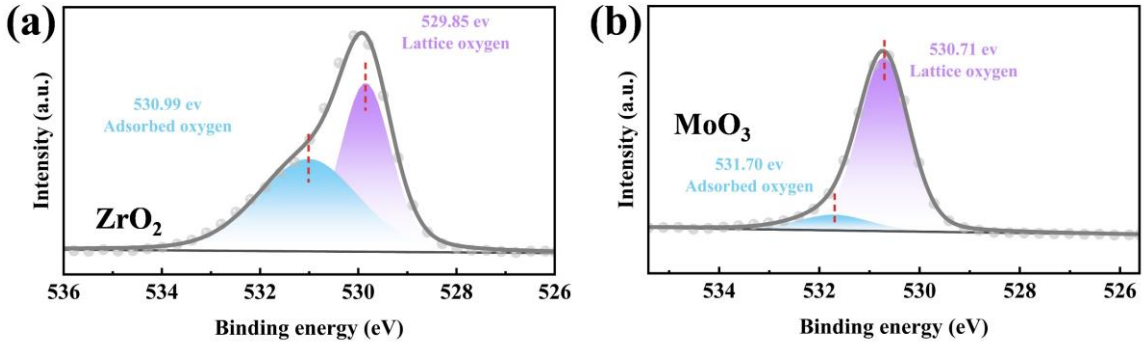

Figure S10. The deconvolution results of XPS spectra of ZrO_2 (a) and MoO_3 (b) for O 1s.

Table S4 A comparison of the elemental contents derived from ICP-OES and XPS.

Catalysts	ICP-OES	XPS			
	Mo Content (%)	Content (%)			
		Zr	Mo	O	
				O_{ads}	O_{lat}
$Mo_{0.08}Zr_{0.8}O_x$-500	8.15	52.9	12.6	9.9	24.6
$Mo_{0.10}Zr_{0.8}O_x$-500	10.34	51.1	14.1	10.0	24.8
$Mo_{0.12}Zr_{0.8}O_x$-500	12.50	50.1	15.9	9.7	24.3
$Mo_{0.20}Zr_{0.8}O_x$-500	18.2	45.2	20.8	9.7	24.3
$Mo_{0.30}Zr_{0.8}O_x$-500	22.65	40.8	25.7	9.4	24.1
$Mo_{0.50}Zr_{0.8}O_x$-500	30.56	18.2	48.1	10.3	23.4
$Mo_{0.10}/Zr_{0.8}O_x$-500-DIM	9.36	46.8	19.7	17.7	15.8

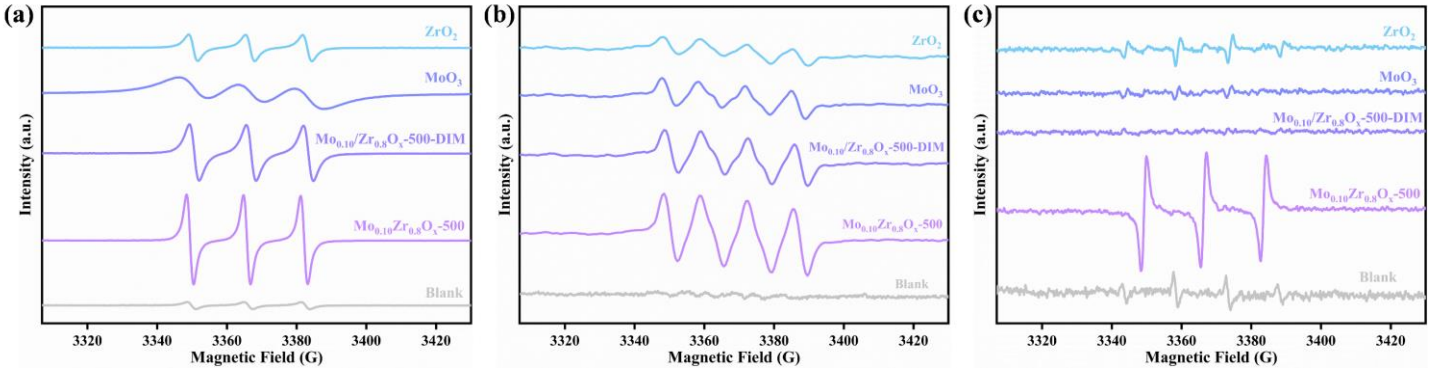

Figure S11. EPR spectra: TEMP trapped $^1O_2$ (a), DMPO-CH_3OH trapped $\bullet O_2^-$ (EPR signals of four large and two small peaks) (b) and DMPO-H_2O trapped •OH (EPR signal intensity ratio: 1:2:2:1) (c) in the presence of $Mo_{0.10}Zr_{0.8}O_x$-500, $Mo_{0.10}Zr_{0.8}O_x$-500-DIM, MoO_3 and ZrO_2.

Text S1 The procedure for the ROS quenching experiments is as follows:

20 mg of $Mo_{0.10}Zr_{0.8}O_x$-500, 1 mmol of methyl phenyl sulfide, and 3 mL of methanol were sequentially added to a 25 mL reaction tube. Subsequently, 0.25 mmol of p-benzoquinone, 50 μL of TEMP, and 0.5 mL of tert-butanol were added to different batches of the experiments to capture $^{\bullet}O_2^-$, $^1O_2$, and •OH, respectively. All other experimental conditions and subsequent treatments were conducted in accordance with standard procedures.

Text S2 The procedure for the EPR trapping experiments is as follows:

In order to obtain precise results, each capture experiment was conducted under quantitative conditions.

In the $^1O_2$ capture experiment, 10 mg of catalyst was initially added to a 7 mL centrifuge tube, followed by the injection of 3 mL of methanol. Subsequently, 50 μL of the spin trapping agent TEMP was added, followed by the rapid addition of 50 μL of a 30% hydrogen peroxide solution. Finally, the centrifuge tube was vigorously shaken for 1 min. Subsequently, the reaction solution was filtered through a nylon filter membrane with a pore size of 0.22 μm into another centrifuge tube. The reaction solution was then aspirated using a capillary tube and sealed, and finally the EPR test was performed.

In the $^{\bullet}O_2^-$ and •OH trapping experiments, 6.25 mg/mL of DMPO-CH_3OH solution and 6.25 mg/mL of DMPO-H_2O solution were prepared in advance for the trapping of $^{\bullet}O_2^-$ and •OH, respectively. The operational parameters were maintained throughout the experiment, with the exception of the replacement of TEMP and methanol in the $^1O_2$ capture experiments with the corresponding trapping agents for $^{\bullet}O_2^-$ and •OH.

The parameters of the EPR instrument utilized in the trapping experiment are as follows: center field strength of 3362 G, sweep width of 150 G, $^1O_2$ receiver gain of 2×10^2, and $^{\bullet}O_2^-$ and •OH receiver gain of 2×10^4.

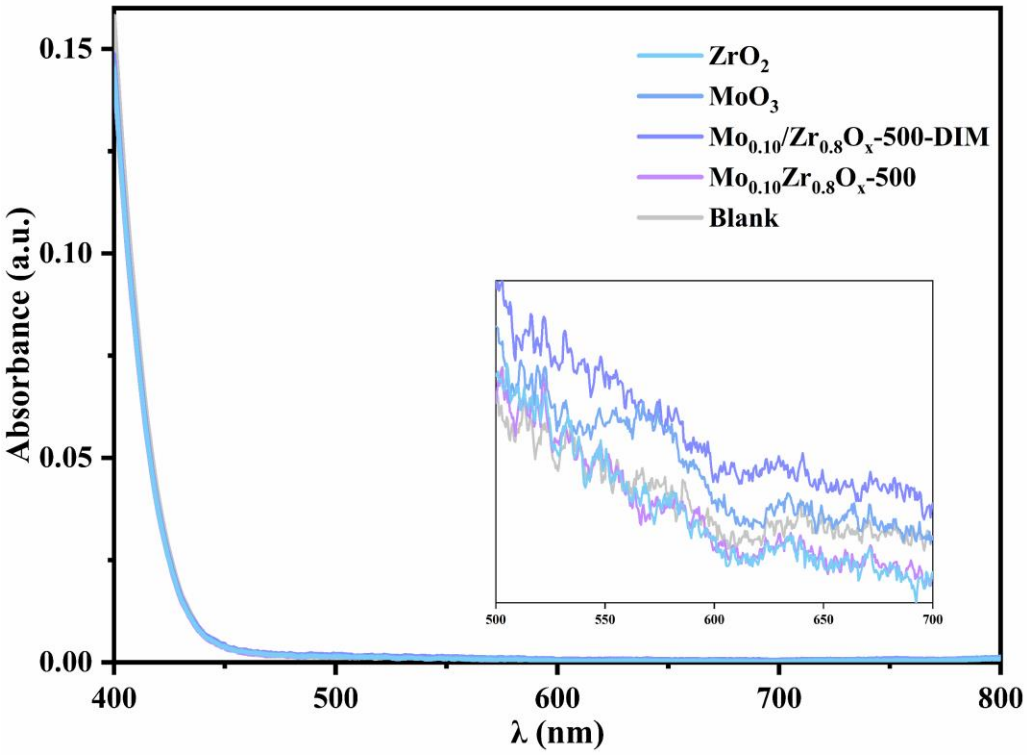

Figure S12. UV-vis absorption spectroscopy of mono-formazan in $Mo_{0.10}Zr_{0.8}O_x$-500/H_2O_2 system.

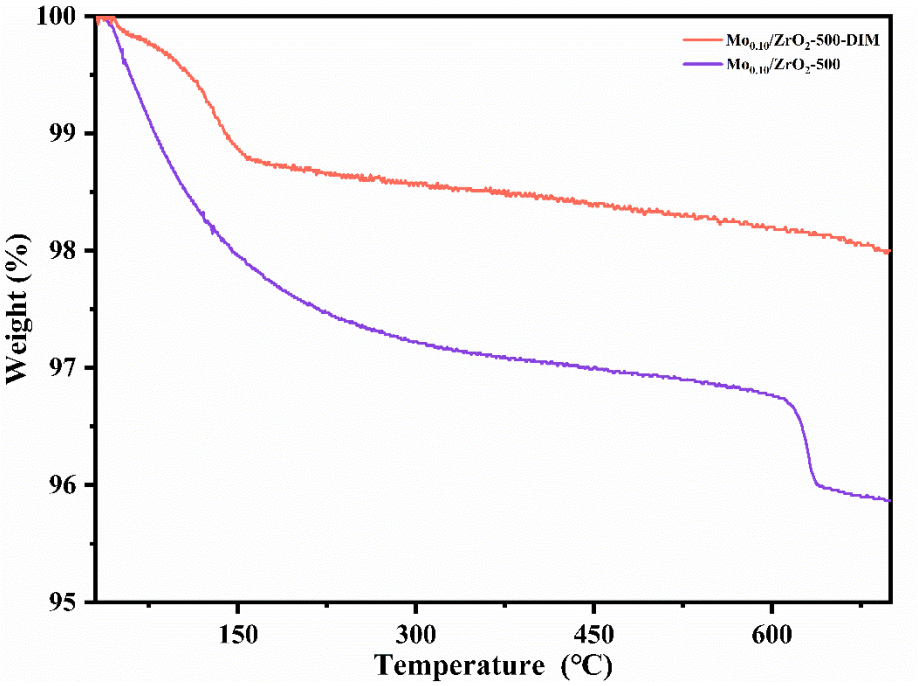

Figure S13. TGA curve of $Mo_{0.10}Zr_{0.8}O_x$-500 and $Mo_{0.10}Zr_{0.8}O_x$-500-DIM.

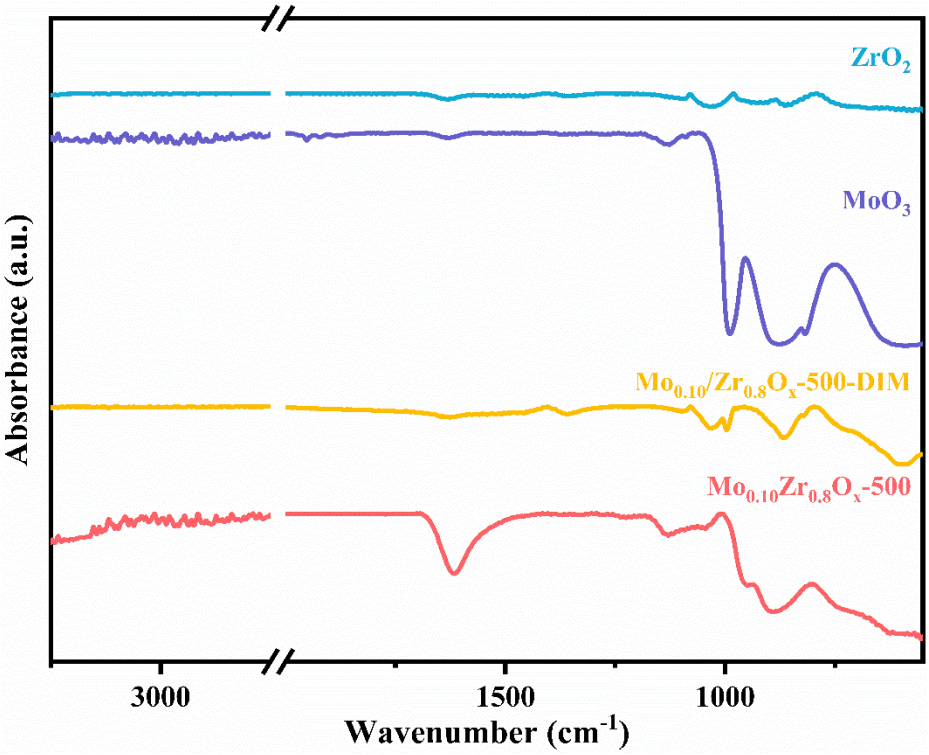

Figure S14. FT-IR spectra of $Mo_{0.10}Zr_{0.8}O_x$-500, $Mo_{0.10}/Zr_{0.8}O_x$-500-DIM, MoO_3 and ZrO_2.

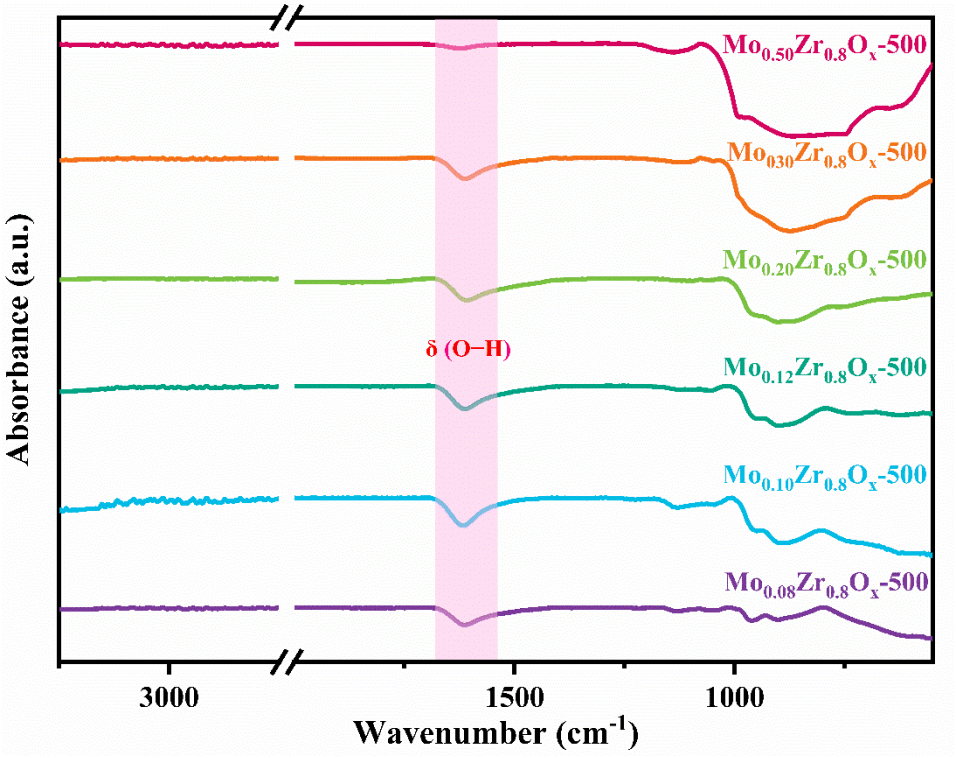

Figure S15. FT-IR spectra of $Mo_{0.08}Zr_{0.8}O_x$-500, $Mo_{0.10}Zr_{0.8}O_x$-500, $Mo_{0.12}Zr_{0.8}O_x$-500, $Mo_{0.20}Zr_{0.8}O_x$-500, $Mo_{0.30}Zr_{0.8}O_x$-500, $Mo_{0.50}Zr_{0.8}O_x$-500

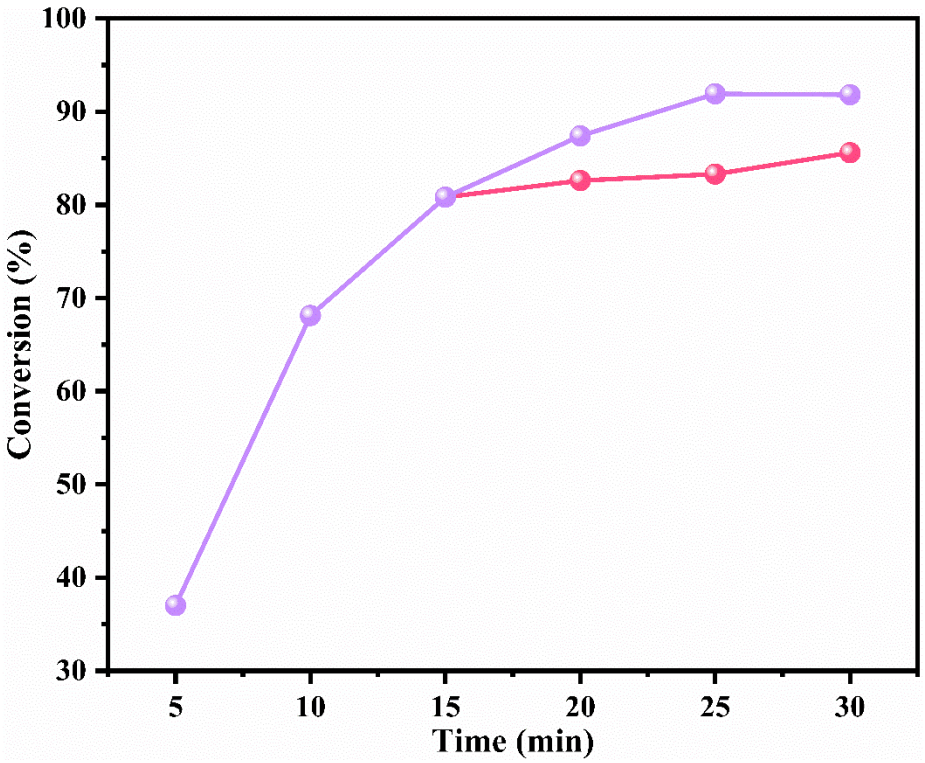

Figure S16. The “hot filtration” experiment.

Table S5 Comparing of $Mo_{0.10}Zr_{0.8}O_x$-500 catalyst with reported catalyst for sulfide oxidation reaction.

Catalyst	Solvent	T (℃)	Time (h)	Oxidant	Conv. (%)	Select. (%)	Yield (%)	Ref.
$Mo_{0.10}Zr_{0.8}O_x$-500	CH_3OH	30	0.5	H_2O_2	98.2	93.5		This work
C8-AP-WO4 = @SBA-15	H_2O:CH_3CN=1:1	30	1.5	H_2O_2			93	[1]
CuL2@Y	CH_3CN	50	6	H_2O_2	81.95	100		[2]
OMS-1-0.40(OAc)	$PhCF_3$	90	4	O_2 (0.1 MPa)		91	87	[3]
PNbMoSi	EtOH	25	4	H_2O_2	92	94		[4]
Fe–TiO_2	CTAB EDC	60	0.5	H_2O_2	80	76		[5]
Cu-Ni-Co	CH_3CN	40	25	H_2O_2			97	[6]
$BaRuO_3$	t-BuOH	40	24	O_2 (1 MPa)		84	92	[7]
$CoFe_2O_4$/Trp/Dy	/	r.t.	50	H_2O_2			92	[8]
CeO_2-Au nanowires	CH_3CN	50	3	H_2O_2	54	100		[9]
Zr-POMs	CH_3CN	27	0.5	H_2O_2	82	89		[10]
La_2O_3	Ethyl acetate	reflux	5	t-BuOOH			88	[11]
ov-Bi_2O_3	Hexane	25	10	O_2 bubble	86	96		[12]

Text S3

According to ICP-OES analysis, the Mo ion content of the reaction filtrate was 9.575 mg/L.

i.e. In the reaction filtrate:

$$\text{Mo Mass} = 9.575\ \text{mg/L} \times 3\ \text{mL} = 0.02873\ \text{mg}$$

$$\text{Mo Content} = \frac{0.02873\ \text{mg}}{20\ \text{mg}} = 0.0014$$

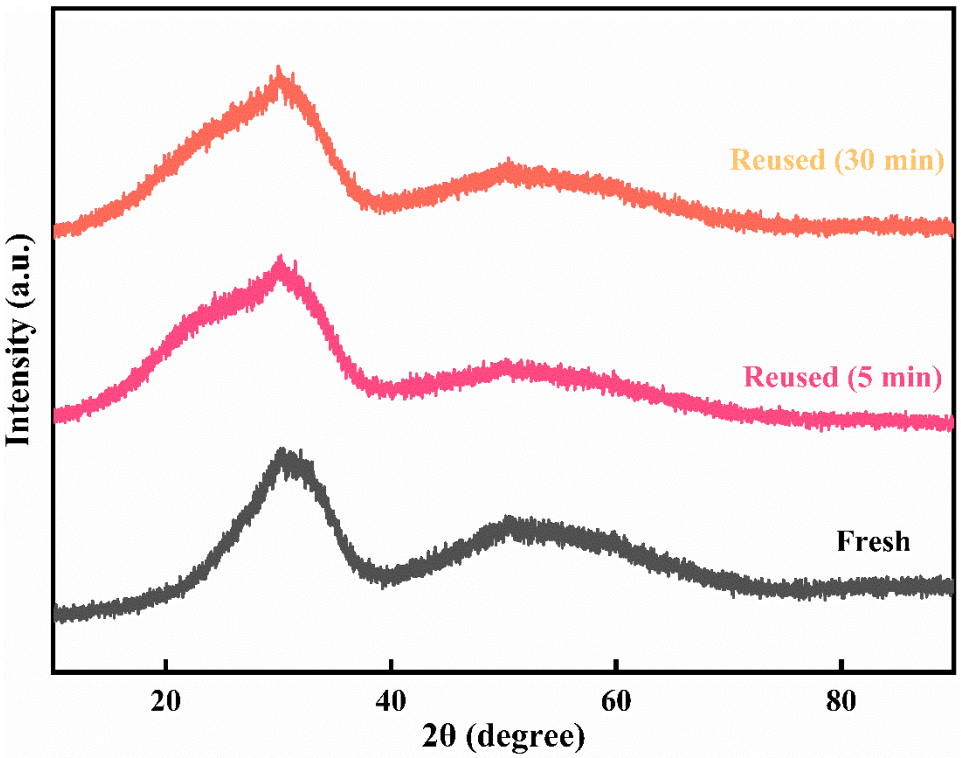

Figure S17. XRD patterns of fresh and reused catalysts (5 min and 30 min).

References

1 B. Karimi and M. Khorasani, Selectivity adjustment of SBA-15 based tungstate catalyst in oxidation of sulfides by incorporating a hydrophobic organic group inside the mesochannels, *ACS Catal.*, 2013, **3**, 1657-1664.

2 B. K. Kundu, M. Das, R. Ganguly, P. A. Bhobe and S. Mukhopadhyay, Role of zeolite encapsulated Cu(II) complexes in electron transfer as well as peroxy radical intermediates formation during oxidation of thioanisole, *J. Catal.*, 2020, **389**, 305-316.

3 M. Koutani, E. Hayashi, K. Kamata and M. Hara, Synthesis and aerobic oxidation catalysis of mesoporous todorokite-type manganese oxide nanoparticles by crystallization of precursors, *J. Am. Chem. Soc.*, 2022, **144**, 14090-14100.

4 M. B. Colombo Migliorero, V. Palermo, G. P. Romanelli and P. G. Vázquez, New niobium heteropolyacid included in a silica/alumina matrix: Application in selective sulfoxidation, *Catalysis Today*, 2021, **372**, 89-97.

5 G. D. Yadav and R. V. Sharma, Synthesis, characterization and applications of highly active and robust sulfated Fe-TiO_2 catalyst (ICT-3) with superior redox and acidic properties, *J. Catal.*, 2014, **311**, 121-128.

6 F. Hosseini-Eshbala, A. Sedrpoushan, M. N. Dehdashti, B. Breit, F. Mohanazadeh and H. Veisi, Needle ball-like nanostructured mixed Cu-Ni-Co oxides: Synthesis, characterization and application to the selective oxidation of sulfides to sulfoxides, *Mater. Sci. Eng., C*, 2019, **103**, 109814pp.

7 K. Kamata, K. Sugahara, Y. Kato, S. Muratsugu, Y. Kumagai, F. Oba and M. Hara, Heterogeneously catalyzed aerobic oxidation of sulfides with a $BaRuO_3$ nanoperovskite, *ACS Appl. Mater. Interfaces*, 2018, **10**, 23792-23801.

8 N. Moeini, S. Molaei and M. Ghadermazi, Dysprosium (III) supported on $CoFe_2O_4$ MNPs as a heterogeneous catalyst for the selective oxidation of sulfides and synthesis of symmetrical disulfides, *J. Mol. Struct.*, 2021, **1246**, 131071.

9 T. F. Rosado, M. P. Teixeira, L. C. Moraes, L. A. d. Silva, A. V. Pontes-Silva, J. G. Taylor, I. C. de Freitas, D. C. de Oliveira, J. Gardener, G. Solorzano, T. V. Alves, M. F. Venancio, M. I. P. da Silva, E. Brocchi, H. V. Fajardo and A. G. M. da Silva, Synergistic effect between CeO_2 nanowires and gold NPs over the activity and selectivity in the oxidation of thioanisole, *Appl. Catal., A*, 2021, **613**, 118010.

10 N. V. Maksimchuk, V. Y. Evtushok, O. V. Zalomaeva, G. M. Maksimov, I. D. Ivanchikova, Y. A. Chesalov, I. V. Eltsov, P. A. Abramov, T. S. Glazneva, V. V. Yanshole, O. A. Kholdeeva, R. J. Errington, A. Sole-Daura, J. M. Poblet and J. J. Carbo, Activation of H_2O_2 over Zr(IV). Insights from model studies on Zr-monosubstituted lindqvist tungstates, *ACS Catal.*, 2021, **11**, 10589-10603.

11 M. Mandal and D. Chakraborty, Kinetic investigation on the highly efficient and selective oxidation of sulfides to sulfoxides and sulfones with t-BuOOH catalyzed by La_2O_3, *RSC Adv.*, 2015, **5**, 12111-12122.

12 J. Wang, X. Xu, Y. Liu, Z. Wang, P. Wang, Z. Zheng, H. Cheng, Y. Dai and B. Huang, Oxygen-vacancy-enhanced singlet oxygen production for selective photocatalytic oxidation, *ChemSusChem*, 2020, **13**, 3488-3494.